Extreme Mechanics Letters 48 (2021) 101446

Contents lists available at ScienceDirect

Extreme Mechanics Letters

journal homepage: www.elsevier.com/locate/eml

Machine learning atomic-scale stiffness in metallic glass

Zheng-Han Peng [a,b], Zeng-Yu Yang [a,c], Yun-Jiang Wang [a,c,*]

[a] State Key Laboratory of Nonlinear Mechanics, Institute of Mechanics, Chinese Academy of Sciences, Beijing 100190, China
[b] College of Materials Science and Engineering, Sichuan University, Chengdu 610065, China
[c] School of Engineering Science, University of Chinese Academy of Sciences, Beijing 100049, China

ARTICLE INFO

Article history:
Received 18 February 2021
Received in revised form 28 June 2021
Accepted 13 July 2021
Available online 19 July 2021

Keywords:
Metallic glass
Machine learning
Atomic stiffness
Molecular dynamics

ABSTRACT

Due to lack of either translational or rotational symmetries at atomic-scale, predicting properties of amorphous materials from static structure is a challenging task. To circumvent the dilemma, a supervised machine-learning strategy via neural network is proposed to predict the atomic stiffness of metallic glass from discretized radial distribution function. The predicted stiffness and its spatial nature are calibrated with molecular dynamics simulations. After which, the origin of atomic constraint is interpreted via the learning structural input. Inadequacy of the model is discussed in terms of incompleteness in both machine-learning configurational space and structural descriptor.

1. Introduction

As a most prevailed paradigm, "structure determines property" has been widely accepted to interpret a material's property in light of structural feature [1,2]. In crystals, dynamics of versatile defects—dislocation, point defect, phase and grain boundary, etc.—can be quantitatively associated with the mechanical responses [3]. However, it is still quite a challenging task to duplicate such a success in amorphous materials, attributing to the lack of periodicity in atomic arrangement [4–6]. The difficulty lies in the fact that there is no intuitive descriptor, in analogy to Brillouin zone in crystals, which is capable of compressing all the structural information, to the maximum extent, into a physics-motivated quantity [7]. Burger's vector of dislocation constitutes another prominent representative of this type.

During the past decades, extensive researches have been devoted to relate structural features with deformation of amorphous materials [8–11]. These structural indicators can be categorized into two groups, i.e., the pure structural ones, and the thermodynamic ones. The formers include coordination number, atomic volume, Voronoi index [12,13], local five-fold symmetry [14,15], two-body entropy [16–18], inversion symmetry breaking [19], and orientational order [20], etc. Then an extended notion of structural signatures with proper thermodynamic input, e.g., soft modes [21,22], vibrational mean-squared displacement [23], flexibility volume [24], local yielding stress [25], and local thermal energy [26] are proposed to forecast particle rearrangement in disordered media. However, these parameters cannot be obtained without the knowledge of inter-particle interactions. Therefore, any function of amorphous material is embedded in the static structures, if one does not be bothered by the complexity of a structural feature [7,27]. Consequently, the open question is how to construct an explicit or hidden law, to connect the disordered structure to property of glasses.

This mission has been pioneered in a set of endeavors to connect atomic position to athermal plastic excitation in amorphous solids, via multiple machine learning (ML) strategies [28–32]. The capacity of artificial intelligence in containing all necessary structural information provides a promising blue print to construct a physically relevant structure–property relationship in amorphous materials [33–37].

Inspired by these ML strategies, we settle an intricate yet important issue in metallic glass (MG), i.e., predicting the atomic-scale stiffness (rigidity), or atomic constraint, which is closely related to a wide range of elasto-plastic deformation mechanisms [9] and the glass transition [38]. A supervised ML protocol via neural network greatly simplifies and facilitates prediction from only the radial distribution function (RDF) of a central atom truncated at different distances as structural input features.

2. Atomistic simulations and machine learning protocol

The supervisory signal—atomic-scale stiffness K—is defined as response of an atom's position to thermal fluctuation:

$$K_i \equiv \frac{k_B T}{\left\langle |\Delta \mathbf{r}_i(\tau)|^2 \right\rangle}. \tag{1}$$

Here $\left\langle |\Delta \mathbf{r}_i(\tau)|^2 \right\rangle$ is the vibrational mean-squared displacement of the ith atom throughout the duration ($\tau = 100$ ps) of a

* Corresponding author at: State Key Laboratory of Nonlinear Mechanics, Institute of Mechanics, Chinese Academy of Sciences, Beijing 100190, China.
E-mail address: yjwang@imech.ac.cn (Y.-J. Wang).

https://doi.org/10.1016/j.eml.2021.101446
2352-4316/

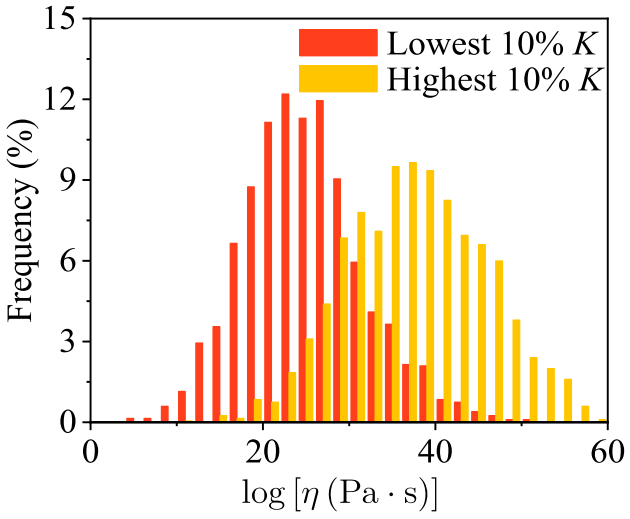

Fig. 1. Distribution of the particle-level viscosity for the 10% atoms with the highest and lowest stiffness in $Cu_{50}Zr_{50}$. Stiffer atoms present larger viscosity and vice versa.

couple of phonon lifetimes at temperature, T. k_B is the Boltzmann constant and k_BT is thermal energy. K_i can be understood as a particle-level spring constant (or elastic modulus) accounting for the cage effect of atoms in glassy environment [38]. The atomic stiffness is closely associated with the propensity of shear transformations as described in Johnson's cooperative shear model [39]. Fig. 1 illustrates the distribution of atomic viscosity for the 10% atoms with the highest and lowest stiffness, respectively, in a $Cu_{50}Zr_{50}$ MG. Stiffer atoms are more viscous that are rigid against thermal fluctuation, and vice versa. In other words, the atomic stiffness distinguishes liquid-like atoms from those in the solid-like elastic matrix. Less stiff atoms are therefore more susceptible to shear instability, and could serve as precursors for shear transformations.

We start with ten independent $Cu_{50}Zr_{50}$ MG samples, each contains 19,652 atoms with dimensions of $\sim 70 \times 70 \times 70$ Å^3. They are quenched from equilibrium liquid with constant cooling rate of 10^{10} K/s. The molecular dynamics (MD) is conducted with LAMMPS [40]. An embedded-atom-method potential is utilized as force field [41]. *NPT* ensemble is enabled with Parrinello–Rahman barostat [42] and Nosé–Hoover thermostat [43]. Periodic boundary conditions are imposed to all directions. The atomic stiffness K_i is calculated as the mean value of the cases from 50 to 300 K with step of 50 K. Activation–relaxation technique nouveau (ARTn) samples the activation energies of local structural excitations [44–46]. For statistical purpose, each atom is activated for 20 times to estimate an average activation energy of viscosity.

The structural descriptor for ML—single-particle RDF is formulated as

$$g_i(r) = \frac{1}{4\pi r^2 \rho \Delta r} \sum_{j=1}^{N} \delta(r - r_{ij}), \tag{2}$$

where $\rho = N/V$ is the number density, with $N = 19652$ and V volume of the simulation box. The summation goes in a shell of thickness $\Delta r = 0.2$ Å with a distance r from the central atom. r is set from 2 to 10 Å with an increment step of 0.2 Å. Such setting guarantees inclusion of the first four shells of RDF, as shown in Fig. 2. The distance is believed to have included full structural environment [27]. Altogether, we obtain 40 structural features as inputs for ML.

Fig. 2 sketches the ML architecture. Artificial neural network is employed to figure out a certain pattern of atomic stiffness via training. Specifically, we choose discretized RDFs as inputs, based on which to establish a quantitative predictive model for local stiffness. The internal parameters of the ML framework are initialized with the normalized initialization process. During training procedure, these parameters are optimized by minimizing the loss function. Specifically, we consider the mean squared error (MSE) as the loss function used in the present work. Here, MSE $= \frac{1}{N}\sum_{i=1}^{N}\left(K_{\text{pre}} - K_{\text{real}}\right)^2$, where K_{pre} and K_{real} denote predicted and real atomic stiffness, respectively. Rectified linear unit (RELU) is used as the activation functions. Here RELU is defined as:

$$f(x) = \begin{cases} x, & \text{if } x > 0 \\ 0, & \text{if } x \le 0, \end{cases} \tag{3}$$

where $f(x)$ and x denote the output and input of a specific unit. We have also tested other activation functions, like sigmoid function as well as tanh function. The result is shown in Fig. S1, which implies that the quality of our ML model is almost insensitive to activation function. Therefore, we chose RELU which presents the simplest form.

The next task is to determine the optimal number of hidden layers and the amount of nodes in each layer. Here, a five-fold cross validation is conducted, on the basis of which, we tested different ML frameworks with various combinations of hidden layers and nodes. The result is shown in Fig. S2 and Table S1. It indicates that one hidden layer framework can definitely achieve excellent predicting capacity and the increment of hidden layers will not dramatically improve the predicting power anymore, but makes the model more complex instead. Besides, the best network which produces the lowest mean-squared error, will arise if we set 200 units in the hidden layer. Therefore, we constructed a optimal ML model with three layers composed, leading to a 40–200–1 architecture, see Fig. 2. Then, during the training process, as we have totally 10 samples, the first nine are used as training sets, and the remaining one is used as testing set.

3. Results and discussion

To evaluate the predictive power, the predicted stiffness K_{pre} is plotted versus the real value (from direction MD simulations) K_{real} in Fig. 3, for both the training and testing set. A strong correlation exists between K_{pre} and K_{real} after coarse-graining with bin size of 100 atoms. The raw data are also shown by the number density. All the coarse-grained data points of stiffness are evenly distributed alone the black line, $y = x$. It is intriguing to see that the agreement in the testing set. With purely static RDF as input, the neural network model enables precise prediction of atomic stiffness, which is comparable to MD. It should be noted that the error is larger at single atomic level when compared with the coarse-grained case. Our explanation to such weak correlation at atomic level is that the intimate correlation between structure and property in amorphous solids is not controlled by the first shell of RDF [27], but rather the materials genome is embedded in several shells of RDF via spatial correlation, implying a non-local scenario of structure–property relationship in amorphous materials [47]. Besides, it has been observed that the prediction is overestimated for large stiffness and underestimated for the low end. This is possibly caused by (1) numerical coarse graining procedure, or (2) The lack of enough extreme situations in the training set, or a combination of (1) and (2).

The machine-learned stiffness can then be transferred to inform other physical properties. First, it is reasonable to assume correlation between K_{pre} and atomic viscosity, η. The latter can be estimated through:

$$\eta_i = \eta_0 \exp\left(\frac{\langle \Delta Q_i \rangle}{k_B T}\right). \tag{4}$$

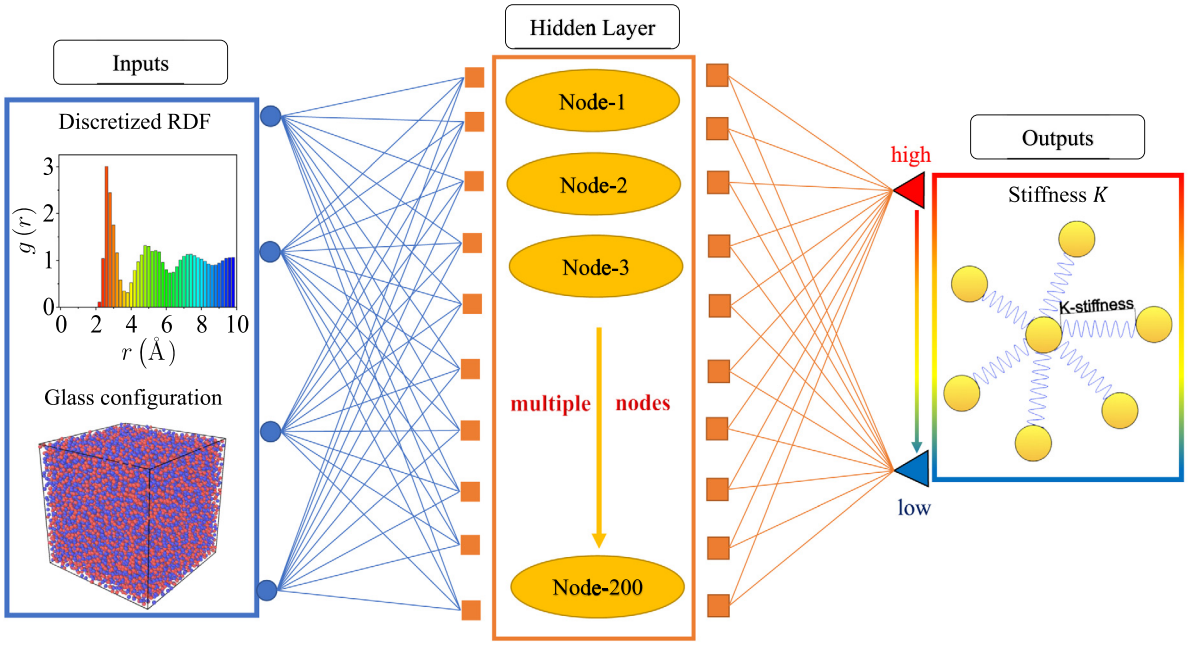

Fig. 2. Framework of the neural network model. Three layers are composed as a network with a 40–200–1 structure: discretized RDF as input, 200 nodes contented in the hidden layer to capture more hidden information, and eventually predicted stiffness of atoms sorted by their magnitude in the output layer. Insets in the first layer show the total RDF and the disordered atomic structure of a glass sample.

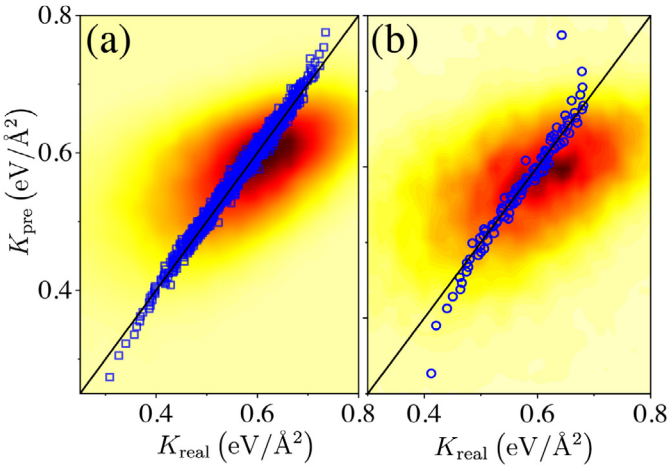

Fig. 3. The machine-learned stiffness K_{pre} as a function of the real value in the (a) training and (b) testing set, respectively. The background color denotes number density. The scattered data are the numerically coarse-grained stiffness with bin size of 100 atoms. The black lines represent prefect prediction, $K_{pre} = K_{real}$. (For interpretation of the references to color in this figure legend, the reader is referred to the web version of this article.)

Here $\eta_0 = 1.0 \times 10^{-4}$ Pa s denotes the high-temperature limit viscosity. $\langle \Delta Q_i \rangle$ is the average activation energy of viscous flow explored by ARTn. The correlation between K_{pre} and η is shown in Fig. 4, where Fig. 4a and b display the raw data and the numerical coarse-grained ones with bin size of 100 atoms, respectively. Viscosity increases exponentially with increasing K_{pre}. It is a strong evidence that viscosity arises from atomic-scale constraint which is in turn totally accommodated by static structure. Up to now, the rule from structure to rigidity remains black-box information. However, we have an opportunity to uncover the structural origin of constraint by examining the input RDF. In Fig. 4c, we plot the RDF of the 10% atoms of the highest and lowest K_{pre} and K_{real}, respectively. The overlap between the scattered points and the solid lines indicates ML has achieved high predictive accuracy. Furthermore, stiffer atoms present RDF of solid-like (glassy) features, i.e., higher first peak and split in the second peak. Meanwhile, the first peak of lower-K atoms moves to shorter distance denoting shrinkage upon glass-to-liquid transition. This demonstrates an opportunity of interpretable ML scheme if the input feature has specific physical meaning.

The ML model is applicable to a wide of disordered configurations. In Fig. 4d we vary the cooling rates from 10^9 K/s to 10^{13} K/s to prepare several more testing sets. Even though the data of different cooling rates does not collapse to $K_{pre} = K_{real}$, the relative value of the stiffness can be figured out in correct order. It means that the dynamical heterogeneity can be distinguished from only RDF. However, we must point out that the rule learned from a specific configurational space—10^{10} K/s in the present case—cannot be extended universally to other cooling conditions. The learning rule overestimates the stiffness of fast-quenched samples, and underestimates the slow-cooled ones. In other words, the topology of a fragment of potential energy landscape (PEL) is cooling rate dependent, and thus, the hidden rule from structure to constraint is variant upon variation in cooling protocol. Consequently, a better ML model with greater predictive power which is invariant to thermal conditions can be reached by broadening the learning space of glass and liquid configurations.

Finally, the spatial nature of atomic constraint can be informed from ML. In Fig. 5, we compare the pattern of ML K_{pre} with that of real stiffness. Since the structure-dynamics correlation is of nonlocal feature, the stiffness have been spatially coarse-grained with dimension of 6 Å (corresponds to the second valley in RDF), which produces optimal correlation. ML yields almost perfect match between K_{pre} and K_{real}. In terms of the spatial distribution of the well-defined atomic stiffness, the liquid-like regions, i.e. these characterized by low atomic stiffness, can be isolated

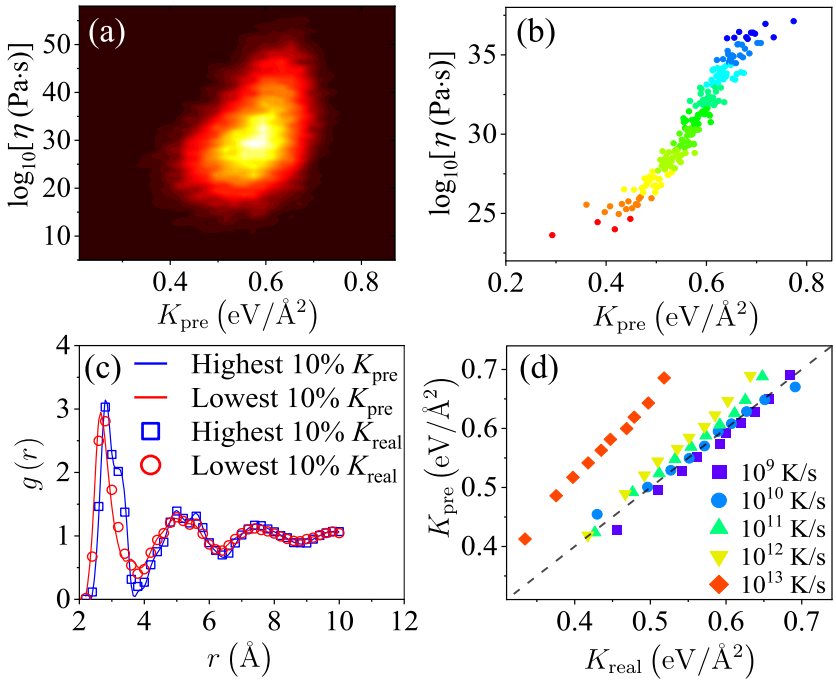

Fig. 4. Characteristics of the machine-learned stiffness. (a)–(b) Viscosity as a function K_{pre} in terms of (a) density map of the raw data and (b) that after coarse graining with bin size of 100 atoms. (c) RDFs of atoms with the 10% highest and 10% lowest K_{pre}, in comparison with those of K_{real}. (d) K_{pre} versus K_{real} at different cooling rates.

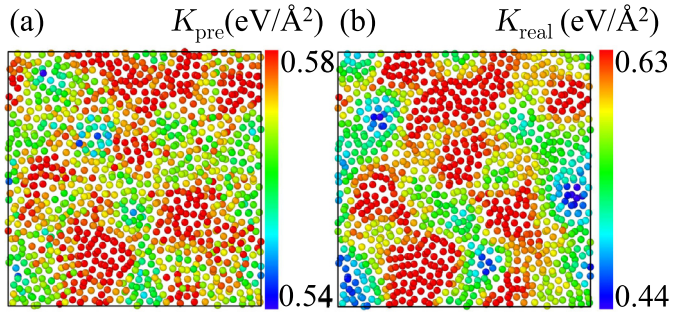

Fig. 5. Spatial nature of the predicted atomic stiffness (a) in comparison with the real value (b). The atoms are colored according to the magnitude of the spatially coarse-grained stiffness (with 6 Å). The shown slice is of 4 Å thickness. (For interpretation of the references to color in this figure legend, the reader is referred to the web version of this article.)

or percolated [48]. Such structural and dynamic heterogeneity of nanometer scale is also in agreement with the reports in literature [49]. Here percolated soft zones will undertake accumulation of small avalanches and thus induce percolation of shear transformations, which eventually leads to homogeneous deformation of metallic glass. In contrast, the isolated modes correspond to the crack-like propagation of plastic deformation which is stress dominated. As a result, severally deformed regions accumulated in narrow regions, causing the formation of shear band in the direction of the maximum shear stress [50,51]. As the K_{pre} is actually the output of static structure, here we further relate structure and plastic deformation in metallic glass. It should be noted that the absolute magnitudes of K_{pre} and K_{real} are not identical to each other. This again demonstrates the inadequacy of the present model—narrow glass configurational space of learning and oversimplified 1D RDF cannot include all topologies in 3D. Moreover, it is of note that the atomic stiffness measured in this work falls in a couple of phonon lifetimes, further research involving long timescale simulations is therefore needed to figure out the connection between local stiffness and diffusive and displacive deformation behaviors of amorphous materials [52,53].

4. Conclusions

In sum, we highlight the importance of artificial intelligence in addressing the intractable prediction of atomic-scale stiffness in metallic glass. A neural network protocol is designed to enable prediction with only atom position correlation (RDF) as structural descriptor. The trained model predicts accurate magnitude of stiffness besides spatial information—the dynamic and structural heterogeneity of nanometer scale—both are of critical significance to amorphous materials. Since RDF is the only input, the model is interpretable, providing a further window to correlate thermodynamic constraint and dynamic viscosity with atomic structure. However, we also note that the present ML model is inadequate due to the lack of full 3D positional information spanning over all disordered space. Inclusion of other physics-motivated thermodynamic and dynamic features might further improve the performance of the ML models.

Declaration of competing interest

The authors declare that they have no known competing financial interests or personal relationships that could have appeared to influence the work reported in this paper.

Acknowledgments

This work is financially supported by the National Key Research and Development Program of China (Nos. 2017YFB0701502 and 2017YFB0702003), the National Natural Science Foundation of China (Nos. 12072344 and 11790292), and the Youth Innovation Promotion Association of Chinese Academy of Sciences, China (No. 2017025).

Appendix A. Supplementary data

Supplementary material related to this article can be found online at https://doi.org/10.1016/j.eml.2021.101446.

References

[1] U.F. Kocks, A.S. Argon, M.F. Ashby, Thermodynamics and kinetics of slip, Prog. Mater. Sci. 19 (1975) 1–278.
[2] A. Argon, Strengthening Mechanisms in Crystal Plasticity, Vol. 4, Oxford University Press on Demand, 2008.
[3] W. Cai, W.D. Nix, Imperfections in Crystalline Solids, Cambridge University Press, 2016.
[4] E.D. Cubuk, R.J.S. Ivancic, S.S. Schoenholz, et al., Structure-property relationships from universal signatures of plasticity in disordered solids, Science 358 (2017) 1033–1037.
[5] C.A. Schuh, T.C. Hufnagel, U. Ramamurty, Mechanical behavior of amorphous alloys, Acta Mater. 55 (2007) 4067–4109.
[6] T.C. Hufnagel, C.A. Schuh, M.L. Falk, Deformation of metallic glasses: Recent developments in theory, simulations, and experiments, Acta Mater. 109 (2016) 375–393.
[7] D. Wei, J. Yang, M.-Q. Jiang, L.-H. Dai, Y.-J. Wang, J.C. Dyre, I. Douglass, P. Harrowell, Assessing the utility of structure in amorphous materials, J. Chem. Phys. 150 (2019) 114502.
[8] F. Spaepen, A microscopic mechanism for steady state inhomogeneous flow in metallic glasses, Acta Metall. 25 (1977) 407–415.
[9] A.S. Argon, Plastic deformation in metallic glasses, Acta Metall. 27 (1979) 47–58.
[10] M.L. Falk, J.S. Langer, Dynamics of viscoplastic deformation in amorphous solids, Phys. Rev. E 57 (1998) 7192.
[11] Y.Q. Cheng, E. Ma, Atomic-level structure and structure–property relationship in metallic glasses, Prog. Mater. Sci. 56 (2011) 379–473.
[12] H.W. Sheng, W.K. Luo, F.M. Alamgir, J.M. Bai, E. Ma, Atomic packing and short-to-medium-range order in metallic glasses, Nature 439 (2006) 419–425.
[13] Y.Q. Cheng, A.J. Cao, E. Ma, Correlation between the elastic modulus and the intrinsic plastic behavior of metallic glasses: The roles of atomic configuration and alloy composition, Acta Mater. 57 (2009) 3253–3267.
[14] H.L. Peng, M.Z. Li, W.H. Wang, Structural signature of plastic deformation in metallic glasses, Phys. Rev. Lett. 106 (2011) 135503.
[15] Y.C. Hu, F.X. Li, M.Z. Li, H.Y. Bai, W.H. Wang, Five-fold symmetry as indicator of dynamic arrest in metallic glass-forming liquids, Nature Commun. 6 (2015) 9310.
[16] D.C. Wallace, On the role of density fluctuations in the entropy of a fluid, J. Chem. Phys. 87 (1987) 2282–2284.
[17] A. Baranyai, D.J. Evans, Direct entropy calculation from computer simulation of liquids, Phys. Rev. A 40 (1989) 3817–3822.
[18] X. Yang, R. Liu, M. Yang, W.-H. Wang, K. Chen, Structures of local rearrangements in soft colloidal glasses, Phys. Rev. Lett. 116 (2016) 238003.
[19] R. Milkus, A. Zaccone, Local inversion-symmetry breaking controls the boson peak in glasses and crystals, Phys. Rev. B 93 (2016) 094204.
[20] J. Yang, Y.-J. Wang, E. Ma, A. Zaccone, L.H. Dai, M.Q. Jiang, Structural parameter of orientational order to predict the boson vibrational anomaly in glasses, Phys. Rev. Lett. 122 (2019) 015501.
[21] A. Widmer-Cooper, H. Perry, P. Harrowell, D.R. Reichman, Irreversible reorganization in a supercooled liquid originates from localized soft modes, Nat. Phys. 4 (2008) 711–715.
[22] J. Ding, S. Patinet, M.L. Falk, Y. Cheng, E. Ma, Soft spots and their structural signature in a metallic glass, Proc. Natl. Acad. Sci. 111 (2014) 14052–14056.
[23] A. Widmer-Cooper, P. Harrowell, H. Fynewever, How reproducible are dynamic heterogeneities in a supercooled liquid?, Phys. Rev. Lett. 93 (2004) 135701.
[24] J. Ding, Y.-Q. Cheng, H. Sheng, M. Asta, R.O. Ritchie, E. Ma, Universal structural parameter to quantitatively predict metallic glass properties, Nature Commun. 7 (2016) 13733.
[25] S. Patinet, D. Vandembroucq, M.L. Falk, Connecting local yield stresses with plastic activity in amorphous solids, Phys. Rev. Lett. 117 (2016) 045501.
[26] J. Zylberg, E. Lerner, Y. Bar-Sinai, E. Bouchbinder, J.S. Langer, Local thermal energy as a structural indicator in glasses, Proc. Natl. Acad. Sci. USA 114 (2017) 7289–7294.
[27] D. Wei, J. Yang, M.-Q. Jiang, B.-C. Wei, Y.-J. Wang, L.-H. Dai, Revisiting the structure–property relationship of metallic glasses: Common spatial correlation revealed as a hidden rule, Phys. Rev. B 99 (2019) 014115.
[28] L. Ward, S.C. O'Keeffe, J. Stevick, G.R. Jelbert, M. Aykol, C. Wolverton, A machine learning approach for engineering bulk metallic glass alloys, Acta Mater. 159 (2018) 102–111.
[29] H. Liu, Z. Fu, K. Yang, X. Xu, M. Bauchy, Machine learning for glass science and engineering: A review, J. Non. Cryst. Solids (2019) 119419.
[30] Q. Wang, A. Jain, A transferable machine-learning framework linking interstice distribution and plastic heterogeneity in metallic glasses, Nature Commun. 10 (2019) 5537.
[31] V. Bapst, T. Keck, A. Grabska-Barwińska, et al., Unveiling the predictive power of static structure in glassy systems, Nat. Phys. 16 (2020) 448–454.
[32] L. Tian, Y. Fan, L. Li, N. Mousseau, Identifying flow defects in amorphous alloys using machine learning outlier detection methods, Scr. Mater. 186 (2020) 185–189.
[33] E.D. Cubuk, S.S. Schoenholz, J.M. Rieser, B.D. Malone, J. Rottler, D.J. Durian, E. Kaxiras, A.J. Liu, Identifying structural flow defects in disordered solids using machine-learning methods, Phys. Rev. Lett. 114 (2015) 108001.
[34] S.S. Schoenholz, E.D. Cubuk, D.M. Sussman, E. Kaxiras, A.J. Liu, A structural approach to relaxation in glassy liquids, Nat. Phys. 12 (2016) 469–471.
[35] E.D. Cubuk, S.S. Schoenholz, E. Kaxiras, A.J. Liu, Structural properties of defects in glassy liquids, J. Phys. Chem. B 120 (2016) 6139–6146.
[36] Z. Fan, J. Ding, E. Ma, Machine learning bridges local static structure with multiple properties in metallic glasses, Mater. Today 40 (2020) 48–62.
[37] X. Liu, X. Li, Q. He, D. Liang, Z. Zhou, J. Ma, Y. Yang, J. Shen, Machine learning-based glass formation prediction in multicomponent alloys, Acta Mater. 201 (2020) 182–190.
[38] B. Li, K. Lou, W. Kob, S. Granick, Anatomy of cage formation in a two-dimensional glass-forming liquid, Nature 587 (2020) 225–229.
[39] W.L. Johnson, K. Samwer, A universal criterion for plastic yielding of metallic glasses with a $\left(T/T_g\right)^{2/3}$ temperature dependence, Phys. Rev. Lett. 95 (2005) 195501.
[40] S. Plimpton, Fast parallel algorithms for short-range molecular dynamics, J. Comput. Phys. 117 (1995) 1–19.
[41] M.I. Mendelev, M.J. Kramer, R.T. Ott, D.J. Sordelet, Molecular dynamics simulation of diffusion in supercooled cu-zr alloys, Phil. Mag. 89 (2009) 109–126.
[42] M. Parrinello, A. Rahman, Polymorphic transitions in single crystals: A new molecular dynamics method, J. Appl. Phys. 52 (1981) 7182–7190.
[43] S. Nosé, A unified formulation of the constant temperature molecular dynamics methods, J. Chem. Phys. 81 (1984) 511–519.
[44] G.T. Barkema, N. Mousseau, Event-based relaxation of continuous disordered systems, Phys. Rev. Lett. 77 (1996) 4358–4361.
[45] R. Malek, N. Mousseau, Dynamics of lennard-jones clusters: A characterization of the activation-relaxation technique, Phys. Rev. E 62 (2000) 7723–7728.
[46] Optimized energy landscape exploration using the ab initio based activation-relaxation technique, J. Chem. Phys. 135 (2011) 034102.
[47] H. Tong, H. Tanaka, Revealing hidden structural order controlling both fast and slow glassy dynamics in supercooled liquids, Phys. Rev. X 8 (2018) 11041.
[48] P. Cao, M.P. Short, S. Yip, Potential energy landscape activations governing plastic flows in glass rheology, Proc. Natl. Acad. Sci. 116 (2019) 18790–18797.
[49] J.C. Qiao, Q. Wang, J.M. Pelletier, H. Kato, R. Casalini, D. Crespo, E. Pineda, Y. Yao, Y. Yang, Structural heterogeneities and mechanical behavior of amorphous alloys, Prog. Mater. Sci. 104 (2019) 250–329.
[50] P. Cao, K.A. Dahmen, A. Kushima, W.J. Wright, H.S. Park, M.P. Short, S. Yip, Nanomechanics of slip avalanches in amorphous plasticity, J. Mech. Phys. Solids 114 (2018) 158–171.
[51] N. Wang, J. Ding, F. Yan, M. Asta, R.O. Ritchie, L. Li, Spatial correlation of elastic heterogeneity tunes the deformation behavior of metallic glasses, Npj Comput. Mater. 4 (2018) 19.
[52] P. Cao, X. Lin, H.S. Park, Strain-rate and temperature dependence of yield stress of amorphous solids via a self-learning metabasin escape algorithm, J. Mech. Phys. Solids 68 (2014) 239–250.
[53] P. Cao, M.P. Short, S. Yip, Understanding the mechanisms of amorphous creep through molecular simulation, Proc. Natl. Acad. Sci. 114 (2017) 13631–13636.